SDR-NNP: Sharpened Dimensionality Reduction with Neural Networks

Youngjoo Kim[†1][a], Mateus Espadoto[†2][b], Scott C. Trager[3][c], Jos B. T. M. Roerdink[1][d] and Alexandru C. Telea[4][e]

[1] *Bernoulli Institute for Mathematics, Computer Science and Artificial Intelligence, University of Groningen, The Netherlands*
[2] *Institute of Mathematics and Statistics, University of São Paulo, Brazil*
[3] *Kapteyn Astronomical Institute, University of Groningen, The Netherlands*
[4] *Department of Information and Computing Sciences, Utrecht University, The Netherlands*
lyoungjookiml@gmail.com, mespadot@ime.usp.br, sctrager@astro.rug.nl, j.b.t.m.roerdink@rug.nl, a.c.telea@uu.nl

Keywords: High-Dimensional Visualization, Dimensionality Reduction, Mean Shift, Neural Networks.

Abstract: Dimensionality reduction (DR) methods aim to map high-dimensional datasets to 2D scatterplots for visual exploration. Such scatterplots are used to reason about the cluster structure of the data, so creating well-separated visual clusters from existing data clusters is an important requirement of DR methods. Many DR methods excel in speed, implementation simplicity, ease of use, stability, and out-of-sample capabilities, but produce suboptimal cluster separation. Recently, Sharpened DR (SDR) was proposed to generically help such methods by sharpening the data-distribution prior to the DR step. However, SDR has prohibitive computational costs for large datasets. We present SDR-NNP, a method that uses deep learning to keep the attractive sharpening property of SDR while making it scalable, easy to use, and having the out-of-sample ability. We demonstrate SDR-NNP on seven datasets, applied on three DR methods, using an extensive exploration of its parameter space. Our results show that SDR-NNP consistently produces projections with clear cluster separation, assessed both visually and by four quality metrics, at a fraction of the computational cost of SDR. We show the added value of SDR-NNP in a concrete use-case involving the labeling of astronomical data.

1 INTRODUCTION

The visual analysis of high-dimensional data is challenging, due to its many observations (also known as points or samples) and values recorded per observation (also known as dimensions, features, or variables) (Liu et al., 2015; Nonato and Aupetit, 2018; Espadoto et al., 2019). Dimensionality reduction (DR), also called projection, is particularly suited for such data. Compared to glyphs (Yates et al., 2014), parallel coordinate plots (Inselberg and Dimsdale, 1990), table lenses (Rao and Card, 1994), and scatterplot matrices (Becker et al., 1996), DR methods scale visually up to thousands of dimensions and hundreds of thousands of samples. DR techniques such as t-SNE (Maaten and Hinton, 2008) and UMAP (McInnes and Healy, 2018), to mention the most popular ones, can segregate *data clusters* into well-separated *visual clusters*, which enables one to reason about the former by seeing the latter, a property generically known as preservation of *data structure* (Behrisch et al., 2018).

A recent survey (Espadoto et al., 2019) noted that many DR techniques score below t-SNE or UMAP in cluster segregation but have other assets – simple usage and implementation, computational scalability, and out-of-sample behavior. Following this, (Kim et al., 2021b) recently proposed Sharpened DR (SDR) to generically improve the cluster segregation ability by sharpening the data prior to DR by a variant of the Mean Shift algorithm (Comaniciu and Meer, 2002). However, SDR is impractical to use as Mean Shift is prohibitively expensive in high dimensions. Separately, Neural Network Projection (NNP) was proposed (Espadoto et al., 2020) to generically imitate any DR technique with good quality, speed, ease-of-use, and out-of-sample ability.

In this paper, we combine the cluster segregation abilities of SDR with the speed, ease-of-use, and out-of-sample abilities of NNP. Our approach jointly addresses the Mean Shift sharpening step of SDR and the generic projection step following afterwards. Our SDR-NNP method has the following features – to our knowledge, not yet *jointly* achieved by existing DR

[a] https://orcid.org/0000-0002-9677-163X
[b] https://orcid.org/0000-0002-1922-4309
[c] https://orcid.org/0000-0001-6994-3566
[d] https://orcid.org/0000-0003-1092-9633
[e] https://orcid.org/0000-0003-0750-0502
[†] These authors contributed equally.

methods:

Quality (C1): We provide better cluster separation than existing DR methods, as measured by well-known metrics in the DR literature;

Scalability (C2): Our method is linear in sample and dimension counts, allowing the projection of datasets of up to a million samples and hundreds of dimensions in a few seconds on commodity GPU hardware;

Ease of use (C3): Our method produces good results with minimal or no parameter tuning;

Genericity (C4): We can handle any real-valued (unlabeled) high-dimensional data;

Stability and out-of-sample support (C5): We can project new samples for a learned projection without recomputing it, in contrast to standard t-SNE and any other non-parametric methods.

We structure this paper as follows: Section 2 discusses related work on dimensionality reduction. Section 3 details our method. Section 4 presents the results that support our above contributions. Section 5 discusses our method. Finally, Section 6 concludes the paper.

2 BACKGROUND

Let $\mathbf{x} = (x^1, \ldots, x^n)$, $x^i \in \mathbb{R}, 1 \leq i \leq n$ be an n-dimensional (nD) real-valued sample, and let $D = \{\mathbf{x}_j\}$, $1 \leq j \leq N$ be a dataset of N samples. A DR technique is a function

$$P : \mathbb{R}^n \to \mathbb{R}^q, \tag{1}$$

where $q \ll n$, and typically $q = 2$. The projection $P(\mathbf{x})$ of a sample $\mathbf{x} \in D$ is a point $\mathbf{p} \in \mathbb{R}^q$. Projecting the whole set D yields a qD scatterplot denoted next as $P(D)$.

DR methods aim to satisfy multiple requirements. Table 1 outlines prominent ones present in several DR surveys (Hoffman and Grinstein, 2002; Maaten and Postma, 2009; Engel et al., 2012; Sorzano et al., 2014; Liu et al., 2015; Cunningham and Ghahramani, 2015; Xie et al., 2017; Nonato and Aupetit, 2018; Espadoto et al., 2019). Besides these, DR techniques also require locality, steerability, and multilevel computation (Nonato and Aupetit, 2018). We do not focus on such additional requirements as these are less mainstream.

The quality (Q) and cluster separation (CS) requirements need additional explanations. Projection quality is assessed by *local* metrics that measure how a small neighborhood of points in D maps to a neighborhood in $P(D)$ and/or conversely. Local quality metrics include the following (see Table 2 for the formal definitions):

Trustworthiness T (Venna and Kaski, 2006): Measures the fraction of close points in D that are also close in $P(D)$. T tells how much one can trust that local patterns in a projection represent actual data patterns. In the definition (Table 2), $U_i^{(K)}$ is the set of points that are among the K nearest neighbors of point i in the 2D space but not among the K nearest neighbors of point i in $\mathbb{R}^n$; and $r(i, j)$ is the rank of the 2D point j in the ordered-set of nearest neighbors of i in $P(D)$;

Continuity C (Venna and Kaski, 2006): Measures the fraction of close points in $P(D)$ that are also close in D. In the definition (Table 2), $V_i^{(K)}$ are the points in the K nearest neighbors of point i in D but not among the K nearest neighbors in 2D; and $\hat{r}(i, j)$ is the rank of the $\mathbb{R}^n$ point j in the ordered set of nearest neighbors of i in D;

Neighborhood Hit NH (Paulovich et al., 2008): Measures how well a projection $P(D)$ separates labeled data, in a rotation-invariant fashion. NH is the number $\mathbf{y}_k^l$ of the k nearest neighbors of a point $\mathbf{y} \in P(D)$, denoted by $\mathbf{y}_k$, that have the same label l as $\mathbf{y}$, averaged over $P(D)$;

Shepard diagram correlation R (Joia et al., 2011): The Shepard diagram is a scatterplot of the pairwise distances between all points in $P(D)$ *vs* the corresponding distances in D. Points below, respectively above, the main diagonal show distance ranges for which false neighbors, respectively missing neighbors, occur. The closer the plot is to the main diagonal, the better the overall distance preservation is. The scatterplot's Spearman rank correlation R measures this – a value $R = 1$ indicates a perfect (positive) distance correlation.

All above metrics are *local*, *i.e.*, capture preservation of data structure in D at the scale given by the neighborhood size K. In practice, what a 'good' K value is for a given dataset D is unknown. K can also vary locally within D as function of the point density. At a higher level, projections are used to reason about the *overall data structure* in D by creating, ideally, visual clusters that are as well separated in $P(D)$ as data clusters are in D, a property called *cluster separation* (CS). High-CS projections show, *e.g.*, how many point clusters exist and how these correlate (or not) with labels or specific attributes (Nonato and Aupetit, 2018), or predict how easy it is to train a classifier for D based on the CS in $P(D)$ (Rauber et al., 2017). In general, it is hard to design objective metrics for CS like one does for local quality, because a 'well separated data cluster' in D is not evident. Hence, CS is typically assessed on (labeled) datasets D for which the ground-truth data-separation is well known, *e.g.*, MNIST (LeCun and Cortes, 2010).

We next discuss existing DR methods in the light of the requirements in Tab. 1. We group these into unsupervised and supervised methods, as follows.

Table 1: Summary of desirable requirements (characteristics) of DR methods.

Requirement name	**Description (the requirement implies that the method has the following properties):**
Quality (Q)	Captures *local* data structures well, as measured by the projection local-quality metrics in Table 2.
Cluster separation (CS)	Captures data structures present at *larger* scales than local structures, *e.g.* clusters, as visual clusters in the 2D scatterplot.
Scalability (S)	Can project datasets of hundreds of dimensions and millions of samples in a few seconds on commodity hardware.
Ease of use (EoU)	Has few (ideally: no) free parameters, which are intuitive and easy to tune to get the desired results.
Genericity (G)	Can project any (real-valued) dataset, with or without labels.
Out-of-sample (OOS)	Can fit new data in an existing projection. OOS projections are also *stable* – small input-data changes cause only small projection changes.

Table 2: Local quality metrics for projections. All metrics range in $[0,1]$ with 0 being lowest, and 1 being highest, quality.

Metric	**Definition**
Trustworthiness (T)	$1-\frac{2}{NK(2n-3K-1)}\sum_{i=1}^{N}\sum_{j\in U_i^{(K)}}(r(i,j)-K)$
Continuity (C)	$1-\frac{2}{NK(2n-3K-1)}\sum_{i=1}^{N}\sum_{j\in V_i^{(K)}}(\hat{r}(i,j)-K)$
Neighborhood hit (NH)	$\frac{1}{N}\sum_{\mathbf{y}\in P(D)}\mathbf{y}_k^l/\mathbf{y}_k$
Shepard diagram correlation (R)	Spearman's rank of $(\|\mathbf{x}_i-\mathbf{x}_j\|, \|P(\mathbf{x}_i)-P(\mathbf{x}_j)\|), 1\leq i\leq N, i\neq j$

Unsupervised methods: Principal Component Analysis (Jolliffe, 1986) (PCA) is simple, fast, out-of-sample (OOS), and easy-to-interpret, also used as pre-processing for other DR techniques that require a moderate data dimensionality n (Nonato and Aupetit, 2018). Being a linear and global method, PCA is deficient on quality and CS, especially for data of high intrinsic dimensionality.

Techniques such as MDS (Torgerson, 1958), Landmark MDS (De Silva and Tenenbaum, 2004), Isomap (Tenenbaum et al., 2000), and LLE (Roweis and Saul, 2000) with its variations (Donoho and Grimes, 2003; Zhang and Zha, 2004; Zhang and Wang, 2007) detect and project the (neighborhood of the) high-dimensional manifold on which data is embedded, and can capture nonlinear data structure. Such methods yield higher quality than PCA, but can be hard to tune, do not all support OOS, and do not work well for high-intrinsic-dimensional data.

Force-directed methods such as LAMP (Joia et al., 2011) and LSP (Paulovich et al., 2008) can yield good quality, good scalability, and are simple to use. However, not all force-directed methods have OOS capability. Clustering-based methods, such as PBC (Paulovich and Minghim, 2006), share many features with force-directed methods, such as good quality, but also lack OOS.

Stochastic Neighborhood Embedding (SNE) methods, like the well-known t-SNE (Maaten and Hinton, 2008), have high overall quality and CS capabilities. Yet, t-SNE has a (high) complexity of $O(N^2)$ in sample count, is very sensitive to small data changes, can be hard to tune (Wattenberg, 2016), and has no OOS. Tree-accelerated t-SNE (Maaten, 2014), hierarchical SNE (Pezzotti et al., 2016), approximated t-SNE (Pezzotti et al., 2017), and various GPU variants of t-SNE (Pezzotti et al., 2020; Chan et al., 2018) improve scalability, but are algorithmically quite complex, and still have sensitivity, tuning, and OOS issues. Uniform Manifold Approximation and Projection (UMAP) (McInnes and Healy, 2018) has comparable quality to t-SNE, is much faster and has OOS. Still, UMAP is also sensitive to parameter tuning.

Autoencoders (AE) (Hinton and Salakhutdinov, 2006; Kingma and Welling, 2013) aim to generate a compressed, low-dimensional representation of the data in their bottleneck layers by training to reproduce the data input at the output. They have similar quality to PCA and are easy to set up, train, and use, are fast, and have OOS capabilities. Self-organizing maps (SOM) (Kohonen, 1997) share with AE the ease of use, training, and computational scalability. Yet, both AE and SOM lag behind t-SNE and UMAP in CS, which is, as explained, essential for interpreting projections.

Supervised methods: ReNDA (Becker et al., 2020) uses two neural networks to implement (1) a nonlinear generalization of Fisher's Linear Discriminant Analysis (Fisher, 1936) and (2) an autoencoder, used for regularization. ReNDA scores well on predictability and has OOS, but needs pre-training of each individual network and has low scalability. Recently, (Espadoto et al., 2020) proposed Neural Network Projections (NNP), where a selected subset $D_s \subset D$ is projected by any DR method to yield a training projection $P(D_s) \subset \mathbb{R}^2$. D_s is fed into a regression neural network which is trained to output a 2D scatterplot that aims to replicate $P(D_s)$. NNP is very fast, simple to use, generic, and has OOS. NNP's major limitation is a lower CS than its training projection.

Semi-supervised methods: The SSNP method (Espadoto et al., 2021) takes a mid path between supervised methods (*e.g.*, NNP) and unsupervised ones (*e.g.*, AE). Like NNP, SSNP has an encoder-decoder architecture with a reconstruction target but adds a classification target using either ground-truth labels from the dataset D or pseudolabels computed from D by a clustering algorithm. SSNP produces 2D projections which look quite similar to those created by our method described next in Sec. 3. However, important differences exist:

- Our method consists of two distinct operations: high-dimensional data sharpening, followed by projection. SSNP only performs the projection step;

- SSNP is a semi-supervised method that relies upon labels or clustering to create the information to learn from. Our method, similar to NNP, uses a t-SNE projection of the data to learn from. This is a fundamental difference between SSNP and our method;
- The architectures of the neural networks for SSNP and our method are fundamentally different. In particular, SSNP uses two different architectures for training, respectively inference. Our method uses a single architecture for both training and inference.
- A key underlying use-case for SDR-NNP is to enhance the separation between unlabeled data clusters so that these can next be labeled by users (see next Sec. 4.3). This is out of scope of SSNP.

Sharpening data: Finding *clusters* of related data points is a key task in data science, addressed by tens of clustering methods (Xu and Wunsch, 2005; Berkhin, 2006). Mean Shift (MS) (Fukunaga and Hostetler, 1975; Cheng, 1995; Comaniciu and Meer, 2002) is particularly relevant to our work. MS computes the kernel density estimation of a dataset D and next shifts points in D upstream along the density gradient. This effectively clusters D, with applications in image segmentation (Comaniciu and Meer, 2002) and graph drawing (Hurter et al., 2012). Recently, Sharpened DR (SDR) (Kim et al., 2021b) used MS for the first time to assist DR: A dataset D is *sharpened* by a few MS iterations, not to be confused with the *clustering* goal of the original MS. The sharpened dataset is next projected by a fast, easy-to-use, stable, but potentially low-CS DR method. Sharpening 'preconditions' the used DR method to overcome its lack of CS. Yet, as MS is very slow for high-dimensional data, this makes SDR impractical for such data.

Table 3 summarizes the DR techniques discussed above and indicates how they fare with respect to the requirements discussed earlier in this section. No reviewed method satisfies all the requirements optimally. We next describe our proposed method SDR-NNP (Table 3 last row) and show that it scores high on these requirements.

Table 3: Summary of DR techniques in Sec. 2 and their characteristics from Table 1.

	Desirable characteristics of the method				
Method	**Q**	**S**	**EoU**	**G**	**OOS**
PCA	low	high	high	high	yes
MDS	mid	low	low	low	no
L-MDS	mid	mid	low	low	no
Isomap	mid	low	low	low	no
LLE	mid	low	low	low	no
LAMP	mid	mid	mid	high	yes
LSP	mid	mid	mid	high	no
PBC	mid	mid	mid	high	no
UMAP	high	high	low	high	yes
t-SNE	high	low	low	high	no
Autoencoder	low	high	high	low	yes
SOM	low	high	high	low	no
ReNDA	mid	low	low	mid	yes
NNP	high	high	high	high	yes
SDR	high	low	mid	high	no
SDR-NNP	**high**	**high**	**high**	**high**	**yes**

3 SDR-NNP METHOD

As outlined in Sec. 2, SDR and NNP have complementary desirable features: SDR produces good cluster separation (CS), while NNP is fast, easy to use, and has OOS ability. Our combined SDR-NNP technique joins these advantages and works as follows (see also Fig. 1). We use SDR to sharpen a small data subset to create an initial 2D projection (Sec. 3.1). Next, we train NNP on the sharpened data and its 2D projection (Sec. 3.2) and use it to project the whole dataset.

3.1 Sharpened Dimensionality Reduction

SDR has two main components, as follows (for full details we refer to (Kim et al., 2021b)):

Sharpening the data: Given a dataset $D \in \mathbb{R}^n$, SDR computes its density using the multivariate kernel density estimator $\rho(\mathbf{x}) : \mathbb{R}^n \to \mathbb{R}^+$ defined as

$$\rho(\mathbf{x}) = \sum_{\mathbf{y} \in N(\mathbf{x})} L\left(\frac{\|\mathbf{x}-\mathbf{y}\|}{h}\right), \tag{2}$$

where $N(\mathbf{x})$ is the set of k_s-nearest neighbors of $\mathbf{x}$ in D; L is a parabolic kernel (Epanechnikov, 1969); and h is the distance of $\mathbf{x}$ to its k_s^{th} (farthest) neighbor in $N(\mathbf{x})$.

Next, SDR shifts points $\mathbf{x} \in D$ using the update rule

$$\mathbf{x}^{next} = \mathbf{x} + \alpha \frac{\nabla \rho(\mathbf{x})}{\max(\|\nabla \rho(\mathbf{x})\|, \varepsilon)}, \tag{3}$$

where $\alpha \in [0,1]$ is a 'learning rate' parameter that controls the shift speed (higher values yield higher speed) and $\varepsilon = 10^{-5}$ is a regularization parameter. After every update (Eqn. 3), the density ρ is computed again using Eqn. 2. This sharpening approach is called Local Gradient Clustering (LGC) by analogy with Gradient Clustering (GC) (Fukunaga and Hostetler, 1975).

SDR has three parameters: t (number of iterations); k_s (number of nearest neighbors); and α (learning rate). We use $k_s \geq 50$ following (Kim et al., 2021b); setting α and t is discussed in Sec. 4.

Projection: SDR produces a dataset D_s which is a sharpened version of the input dataset D. SDR next projects D_s by a DR method of choice (typically fast but not necessarily OOS), called the *baseline* DR method below, to obtain a 2D projection $P(D_s)$. The data in D_s are better separated than in D, which allows a projection P to produce better cluster separation in $P(D_s)$ than in $P(D)$.

3.2 Training NNP

The key idea of SDR-NNP is to use SDR (Sec. 3.1) on a *small* data subset to obtain $P(D_s)$. To project the full dataset D, we next train the NNP regressor (Espadoto et al., 2020) using D_s as the high-dimensional input and $P(D_s)$ as the 2D output. The network has three fully-connected hidden layers with ReLU activation (Agarap, 2018), initial weights set to He Uniform (He et al., 2015), and an initial bias value set to 0.0001. The output layer has 2 units, one per 2D coordinate, and uses sigmoid activation to constrain output values to $[0,1]$. We used three different network sizes, namely, *x-small* (75, 30, 75 units per layer), *small* (150, 60, 150 units per layer) and *medium* (300, 120, 300 units per layer). We trained the network using the ADAM optimizer (Kingma and Ba, 2014), as described in the NNP paper.

After training, we have a regressor able to mimic the behavior of SDR for unseen data, thus adding stability, OOS capability, and computational scalability to SDR.

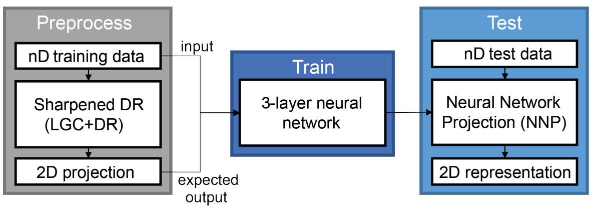

Figure 1: Architecture of the SDR-NNP pipeline.

4 RESULTS

We measured the performance of SDR-NNP by the four metrics in Tab. 2 computed for $K = 7$, in line with (Maaten and Postma, 2009; Martins et al., 2015; Espadoto et al., 2019). Note that K, the number of nearest neighbors used to compute the metrics in Tab. 2, is smaller than k_s, the number of nearest metrics used to evaluate L (Eqn. 2). Indeed, k_s needs to be relatively large to smooth out local noise in the computation of the gradient $\nabla\rho$; in contrast, K is typically set small to capture more local quality aspects of a projection.

Evaluation used six publicly available real-world datasets (Table 4), all being reasonably high-dimensional and large (tens of dimensions, thousands of samples), and with a non-trivial data structure. All dimensions were rescaled to the $[0,1]$ range, to match NNP's sigmoid activation function used in its output layer (Sec. 3). All computed metrics can be found in the Appendix.

Section 4.1 details the quality of SDR-NNP trained to mimic SDR in combination with Landmark MDS (LMDS), PCA, and t-SNE. Section 4.2 studies the computational scalability of SDR-NNP. Finally, Section 4.3 presents an application of SDR-NNP to the analysis of an astronomical dataset.

4.1 Quality on Real-World Datasets

We studied SDR-NNP's quality with respect to its parameters (number of iterations t, learning rate α, training epochs E, and NNP network size) using LMDS, t-SNE, and PCA as baseline DR methods. A discussion on the selection of DR methods for SDR can be found in Sec. 6 from (Kim et al., 2021b). For space reasons we omitted results for all network sizes other than *medium*.

Figure 2 shows how the number of iterations t affects the sharpening of clusters for LMDS and t-SNE (PCA results omitted for space reasons). For all datasets, 4 to 8 iterations suffice to have the clusters sharply defined in the projection. Table 7 in the Appendix shows quality metrics as functions of t for all three baseline projections. Increasing t can increase quality (Air Quality, Reuters with LMDS and PCA) but generally slightly decreases quality for LMDS and PCA. For t-SNE, this decrease is visible for all datasets, which is explainable by the fact that t-SNE already has a very high quality which is hard to be learned by NNP (see (Espadoto et al., 2020)). However, as already argued in (Kim et al., 2021b), local quality metrics will likely decrease when using SDR to favor visual cluster separation.

Figure 3 shows results for SDR-NNP when varying the learning rate α for LMDS and t-SNE (PCA results omitted again for space reasons). Too small or too large α values tend to affect the scatterplot adversely. Values in the range $\alpha \in [0.05, 0.1]$ show the best results, *i.e.*, a good separation of the projection into distinct clusters. Table 8 in the Appendix shows quality metrics as function of α for all three baseline projections. The effect of α on quality is similar with that of t with some combinations (Reuters with LMDS and PCA) showing a slight increase but most showing a slight decrease for small α values.

Figure 4 shows how the number of training epochs E affects projection quality. The early stopping strategy proposed in the NNP paper (Espadoto et al., 2020), which stops training on convergence, defined as the epoch where the validation loss stops decreasing (roughly $E = 60$ epochs in practice), does not produce good results for SDR-NNP – the resulting projection (Fig. 4a,b leftmost columns) show a fuzzy version of the training projection (Fig. 4a,b rightmost columns). This is explained by the fact that SDR-NNP needs to

Table 4: Datasets used in SDR-NNP's evaluation.

Dataset name and provenance	**Samples** N	**Dimensions** n	**Data description**
Air Quality (Vito et al., 2008)	9358	13	Measurements from air sensors used to study and predict air quality
Concrete (Yeh, 1998)	1030	8	Measurements of chemico-physical properties of concrete used to study concrete strength
Reuters (Thoma, 2017)	5000	100	Attributes extracted from news report documents using TF-IDF (Salton and McGill, 1986), a standard method in text processing. This is a subset of the full dataset which contains data for the six most frequent classes only. Used to study how features can predict news' types (classes)
Spambase (Hopkins et al., 1999)	4001	57	Text dataset used to train email spam classifiers
Wisconsin (Street et al., 1993)	569	32	Features extracted from images of breast masses used to detect malignant cells
Wine (Cortez et al., 2009)	6497	11	Samples of white and red Portuguese *vinho verde* used to describe perceived wine quality

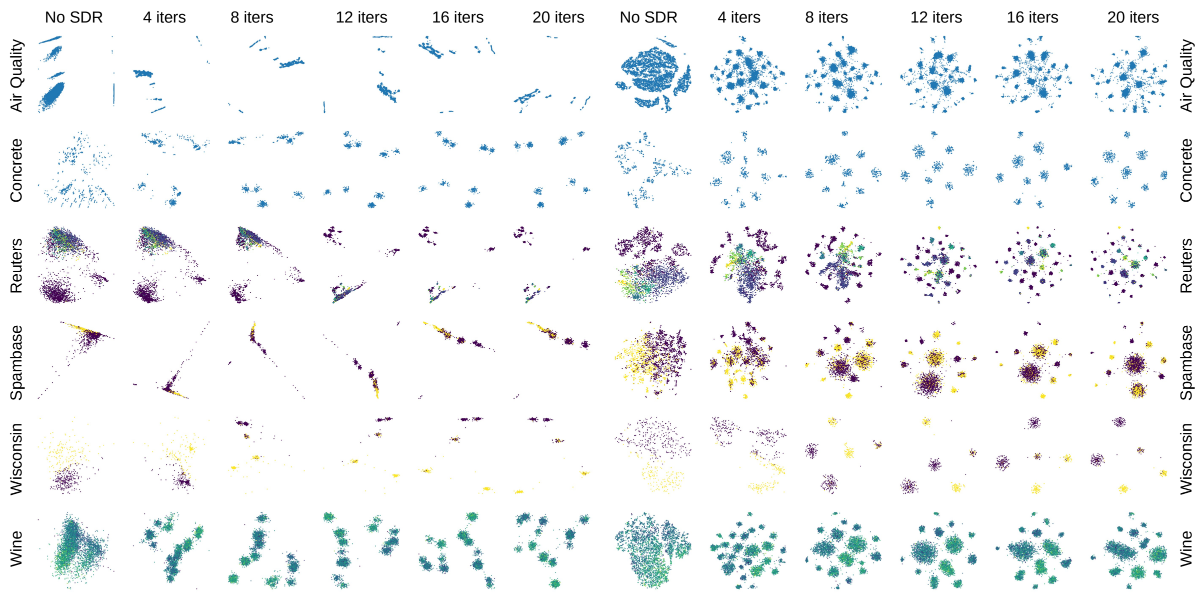

(a) LMDS (b) t-SNE

Figure 2: Iteration parameter effect: SDR-NNP learned from LMDS (a) and t-SNE (b) for varying iterations t (columns) and datasets (rows). Fixed SDR-NNP parameters are $\alpha = 0.1$, $E = 1000$ epochs, *medium* network size.

Table 5: Time measurements for SDR and SDR-NNP (seconds), GALAH dataset. See also Fig. 6.

Samples	**SDR**	**SDR-NNP inference**
1000	0.220	0.108
2000	0.957	0.059
5000	14.799	0.092
10000	157.420	0.149
20000	1302.268	0.414
30000	4736.995	0.355
40000	11058.267	0.727

learn *both* the data sharpening and the projection P, which needs more effort than learning just the projection, as NNP did. If we use more training epochs, Fig. 4 shows that SDR-NNP can reproduce the training projection very faithfully. SDR-NNP produces good results with as little as $E = 300$ epochs, except for the Air Quality dataset, where $E = 3000$ epochs was needed for best results. On average, $E = 1000$ epochs produced visually good results for all datasets and other parameter settings, so we choose this as a preset value for E.

The projections in Figs. 2–4 deserve some comments. As visible there, varying the t and α parameters can create artificial *oversegmentation* – the appearance of many small clusters in the projection, which is an artificial cluster separation (CS), see *e.g.* Fig. 3b, Reuters, $\alpha \geq 0.1$. This effect is strongest, and undesirable, for baseline projections which already do have a good CS, such as t-SNE. In contrast, for projections with a low CS, such as LMDS, artificial oversegmentation is far less present. Like SDR, SDR-NNP is best used when combined with baseline DR methods with a *low* CS capability.

Separately, as outlined in (Kim et al., 2021b), SDR performs best, and is meant to be used for, datasets that are known to have cluster structures since sharpening, by construction, will enhance these structures (Comaniciu and Meer, 2002). SDR-NNP inherits

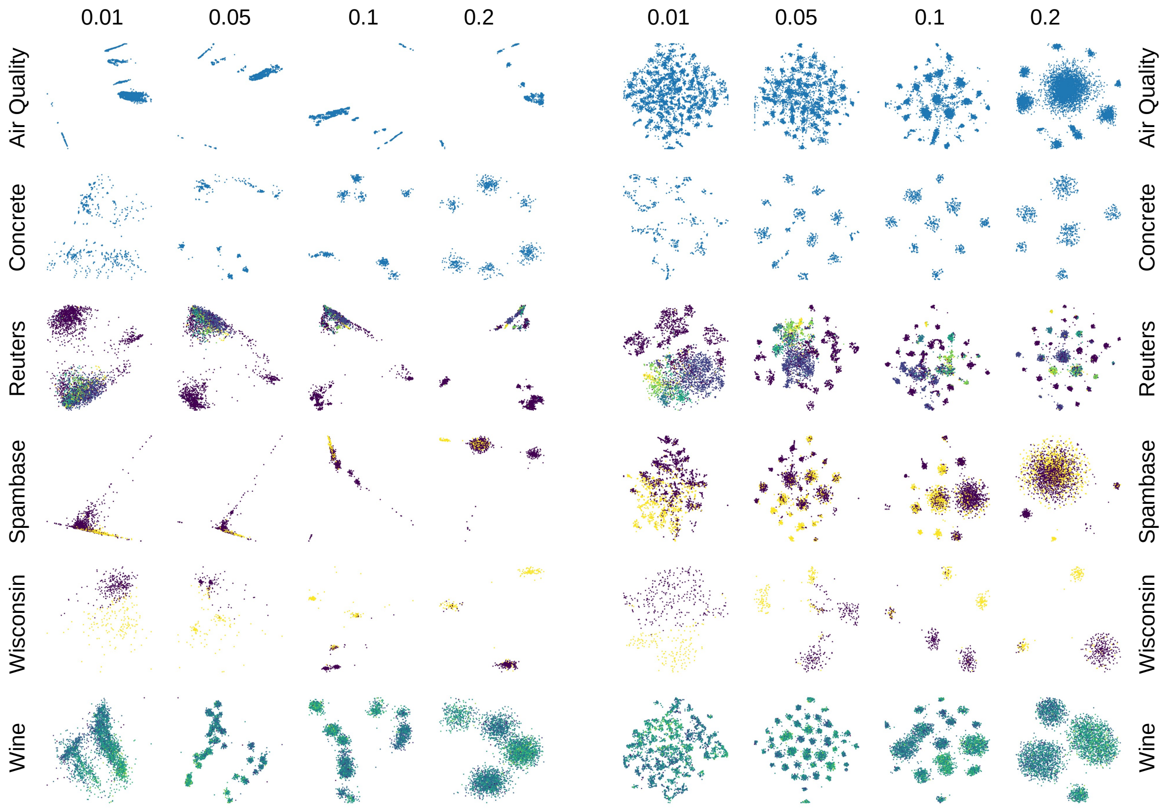

(a) LMDS (b) t-SNE

Figure 3: Learning rate effect: SDR-NNP learned from LMDS (a) and t-SNE (b) for varying learning rates α (columns) and datasets (rows). Fixed SDR-NNP parameters are $t = 10$ iterations, $E = 1000$ epochs, *medium* network size.

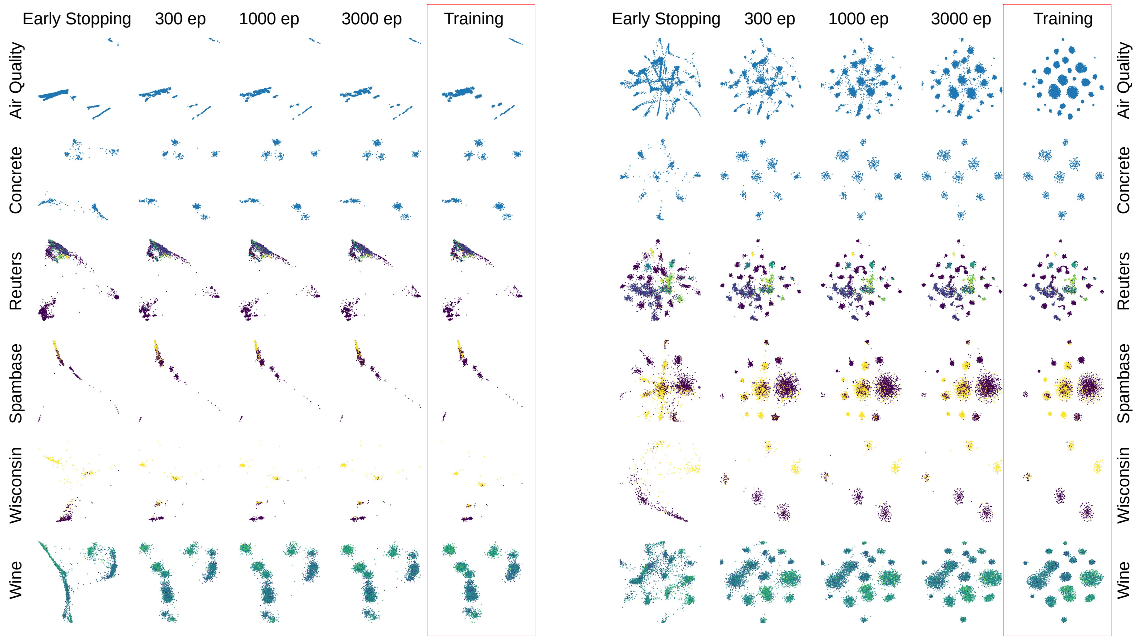

(a) LMDS (b) t-SNE

Figure 4: SDR-NNP learned from LMDS (a) and t-SNE (b) for varying training epochs E (columns) and datasets (rows). Fixed SDR-NNP parameters are $t = 10$, $\alpha = 0.1$, *medium* network size. Red column shows the training projections.

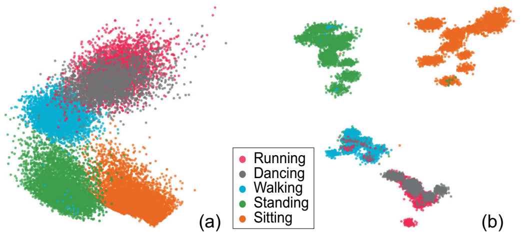

Figure 5: (a) LMDS and (b) SDR with LMDS baseline ($\alpha = 0.2$, $t = 10$, $k_s = 100$) applied to Human Activity Data (N=24075, n=60), which was originally tested by Kim *et al.* (Kim et al., 2021b). Points are colored by their labels on different human activities (sit, stand, walk, run, and dance). These results demonstrate the advantage of using sharpening for data that are known to have cluster structures.

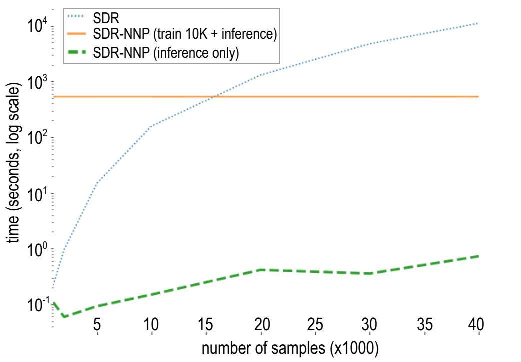

Figure 6: Performance of SDR *vs* SDR-NNP on the GALAH dataset (time in log scale), 1K to 40K samples. SDR-NNP trained with 10K samples for 1000 epochs. See also Tab. 6.

these aspects from SDR and, as Fig. 4 shows, can reproduce SDR highly accurately, and is much faster (see next Sec. 4.2).

To clarify the above, Fig. 5 shows an example where SDR shows far better CS compared with a baseline DR method (LMDS) when applied to real-world human activity data, which is *known* to have distinct and well separated features among different human motions (sit, stand, walk, run, and dance) (El Helou, 2020). Even though the points are known to be well-separated, LMDS produces a relatively low CS (clusters overlap in Fig. 5a). In contrast, SDR produces a much higher CS (Fig. 5b), in line with the ground truth. A second example illustrating the same point is discussed in detail in Sec. 4.3.

4.2 Computational Scalability

We measured scalability by comparing the execution time of the original SDR method with SDR-NNP using samples from the GALAH dataset (described next in Sec. 4.3) with increasing sizes, namely, 1K, 2K, 5K, 10K, 20K, 30K, and 40K samples. Using more samples was not practical since SDR already took over three hours at 40K samples. Figure 6 and Table 5 show these figures. For $|D_s| = 10K$ training samples and $E = 1000$ epochs, SDR-NNP takes considerable time to train, *i.e.*, 372.818 seconds (Fig. 6, orange line). Still, this is already faster than SDR for 15K samples.

In inference mode (after training), SDR-NNP is orders of magnitude faster than SDR, taking less than *one second* to project 40K samples (Fig. 6, green curve). SDR takes *over three hours* for the same data size (Fig. 6, blue curve).

4.3 Case Study: Astronomical Datasets

We applied SDR-NNP to a practical use-case using real-world astronomical data. We use here the same subset of 10K samples from the GALactic Archaeology with HERMES survey (GALAH DR2) (Buder *et al.*, 2018) as in Kim *et al.* to show that our method can create similar projections to their SDR method. The original GALAH DR2 dataset consists of various stellar abundance attributes of 342682 stars. Data cleaning followed (Kim et al., 2021b): first, cross-match the star ID of GALAH DR2 with *Gaia* data release 2 (Gaia DR2) to gain additional information on the stellar kinematics (i.e., 6D phase-space coordinates–x, y, z, u, v, and w) (Buder *et al.*, 2018; Gaia Collaboration, 2016; Gaia Collaboration, 2018); next, exclude stars with implausible values (exceeding 25K parsec in x, y, and z attributes), having unreliable stellar abundances, or have missing values in any dimension. From the remaining 76270 samples after preprocessing, we took the same subset D of 10K stars as in (Kim et al., 2021b), where stars were randomly selected, and compute SDR and the training projection with the same $\alpha = 0.18$ (see Sec. 3.1). We trained SDR-NNP on these 10K stars and used the trained network to project the remaining 66270 samples.

Figure 7 shows SDR-NNP applied to the 66K test data with LMDS and t-SNE as baseline DR methods. Points are colored based on the value of the attribute [Fe/H], which is of interest to domain experts to explain possible data clusters. The first four columns show the SDR-NNP results for varying training epoch counts E. The red column shows the training projection $P(D_s)$ of 10K samples. We see that the structure of the training projection (four clusters) is well reflected by the SDR-NNP results from $E = 300$ epochs onwards. The test projections are more fuzzy, but this is expected, as these contain 66K *unseen* samples which, albeit drawn from the same dataset, cannot perfectly match the four clusters determined by the 10K training samples. The rightmost column in Fig. 7 shows the result of the 'raw' NNP method, *i.e.*, trained to imitate LMDS, and t-SNE, *without* the sharpening step of SDR, respectively. These results show clearly far less cluster separation (CS) than either the SDR-NNP training projection (red column) or the inferred SDR-NNP projections (leftmost four columns). This demonstrates the added value of the *sharpening* step: without it, NNP, albeit fast and OOS-capable, cannot produce useful projections. Table 6 in the Appendix shows quality metrics corresponding to the images in Fig. 7 which support the above observations.

The fact that SDR-NNP shows a good cluster separation allows astronomers to easily label clusters and perform further analysis to infer the physical meaning of stars. To demonstrate this, we manually labeled the clusters from the SDR-NNP plot learned from LMDS to reproduce the same analyses made by Kim *et al.* (Fig. 10 in (Kim et al., 2021b)) to understand the origin and location of the stars in each cluster. Figure 8a shows the manually labeled clusters by one of the authors (astronomy expert). Stars from class 5 are separately labeled as outliers. Figures 8b,c are the Tinsley diagram (Tinsley, 1980) and the copper abundance of the stars – a tracer of supernovae type 1a – as a function of their iron abundance, respectively. From these plots, astronomers are able to identify class-1 stars as thin-disk stars, class-2 stars as metal-rich thick disk stars, class-3 and class-5 (outlier) stars as the normal thick disk stars, and class-4 stars as Gaia Enceladus (GES) – a group of stars that originated from a galaxy that merged with the Milky Way several billions years ago. Importantly, the original SDR method was not able to perform this analysis and identify class-4 stars since it could not be applied to the entire dataset due to its prohibitively low speed.

4.4 Implementation details

All experiments were run on a dual 16-core Intel Xeon Silver 4216 at 2.1 GHz with 256 GB RAM and an NVidia GeForce GTX 1080 Ti GPU with 11 GB VRAM. SDR was implemented in C++ using Eigen (Guennebaud et al., 2010) for matrix computations, Nanoflann (Blanco and Rai, 2014) for nearest-neighbor search, and the implementations of t-SNE and Landmark MDS from Tapkee (Lisitsyn et al., 2013). NNP is implemented using the Keras framework (Chollet and others, 2015). The SDR-NNP code, datasets, and all results discussed above are publicly available at (Kim et al., 2021a).

5 DISCUSSION

We discuss how SDR-NNP performs with respect to the criteria laid out in Sec. 1.

Quality (C1): SDR-NNP is able to create projections which are very similar visually, but also in terms of quality metrics, to those created by SDR. Importantly, the strong separation of similar-valued samples, the key property that SDR promoted, is retained by SDR-NNP. Combined with properties C2–C4 (which SDR does not have), this makes SDR-NNP superior to SDR. Compared to NNP used on the unsharpened data (Fig. 7), SDR-NNP shows significantly better cluster separation, which makes it superior to NNP.

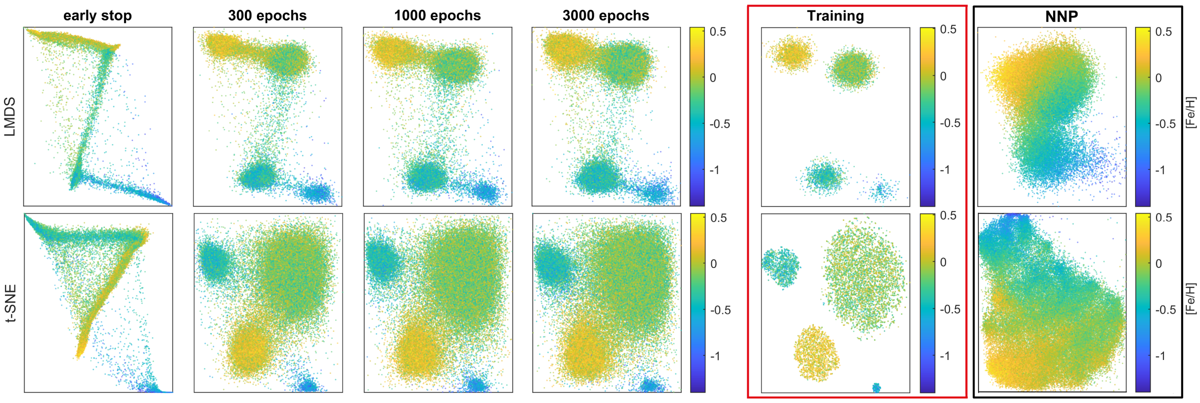

Figure 7: SDR-NNP of 66K samples learned from LMDS (top) and t-SNE (bottom) for different numbers of training epochs E (four leftmost columns). SDR-NNP parameters are $t = 10$ iterations, $\alpha = 0.18$, and *medium* network size. Red column: training projection (10K samples). Rightmost column: NNP trained with LMDS and t-SNE instead of SDR applied to the same test data.

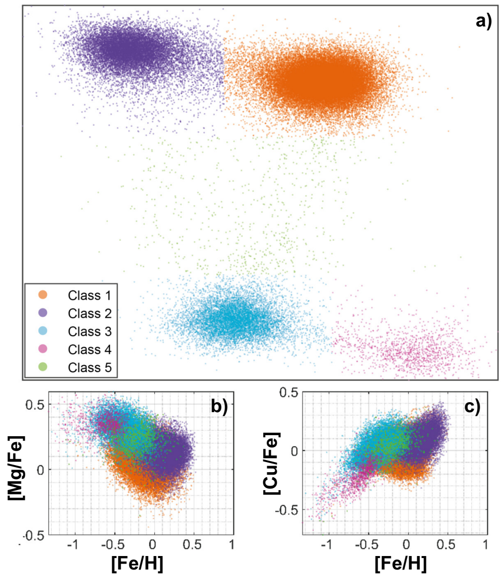

Figure 8: Analysis of GALAH DR2 with SDR-NNP learned from LMDS. (a) Labeling of clusters (classes 1–4) and outliers (class 5). (b) Tinsley diagram and (c) copper abundance of stars *vs* their iron abundance. Astronomers can infer from (b,c) that class 1 is mostly thin disk stars, class 2 is mostly metal-rich thick disk stars, classes 5 and 3 are normal thick disk stars, and class 4 is the Gaia Enceladus (GES) in the Milky Way.

Scalability (C2): SDR-NNP is faster than SDR alone from roughly 15K samples onwards, even when considering training time. In inference mode (after training), SDR-NNP is several orders of magnitude faster than SDR, being able to project tens of thousands of observations in under a second on a high-end PC. Importantly, SDR-NNP's speed is *linear* in the number of dimensions and samples (a property inherited from the NNP architecture), and can handle samples in a *streaming* fashion, one at a time, *i.e*, does not need to hold the entire high-dimensional dataset in memory. This makes SDR-NNP scalable to large datasets of millions of samples.

Ease of use (C3): Once trained, SDR-NNP is parameter-free. The influence of its hyperparameters t (sharpening iterations), E (number of training epochs), and α (learning rate) is detailed in Sec. 4.1. The preset $t = 10, E = 1000, \alpha \simeq 0.2$ was shown to give good results for the entire range of tested datasets.

Genericity (C4): SDR-NNP is agnostic to the nature and dimensionality of the input data, being able to project any dataset having quantitative variables. Tables 6, 7, and 8 in the Appendix show that SDR-NNP achieves high quality on datasets of different nature and coming from a wide range of application domains (air sensors, civil engineering, text mining, imaging, and chemistry).

Stability and out-of-sample support (C5): SDR-NNP inherits the stability and OOS support of NNP, making it possible to train on a small subset of a given dataset and then stably project the remaining data drawn from the same distribution.

Limitations: While inheriting the abovementioned desirable properties from NNP, SDR-NNP also inherits some of its limitations. Its OOS support cannot extend to datasets of a completely different nature than those it was trained on – arguably, a limitation that most machine learning methods have. Also, SDR-NNP is only as good as the baseline projection P that was used in the SDR phase. Using a poor quality projection leads to SDR-NNP learning, and reproducing, that behavior. Separately, SDR-NNP learns to imitate the sharpening behavior of SDR. While this is of added value in identifying data structure in terms of visual structure, as shown by the results in Sec. 4, applying SDR-NNP on a dataset with little or no cluster structure can create artificial visual oversegmentation in the projection (see Sec. 4.1). The recommended parameter values to prevent oversegmentation using SDR are discussed further in Sec. 6.5 in (Kim et al., 2021b). Specifying the right amount of sharpening is dataset- and problem-dependent, thus considered as future work.

6 CONCLUSION

We have presented SDR-NNP, a new method for computing projections of high-dimensional datasets for visual exploration purposes. Our method joins several desirable, and complementary, characteristics of two earlier projection methods, namely NNP (speed, ease of use, out-of-sample support, ability to imitate a wide range of existing projection techniques with a high quality) and SDR (ability to segregate projections of complex datasets into visually separated clusters of similar observations). In particular, SDR-NNP removes the main obstacle for practical usage of SDR, namely, its prohibitive computational time. We have demonstrated SDR-NNP on a range of datasets coming from different application domains. In particular, we showed how SDR-NNP can bring added value in the exploration of a large and recent astronomical dataset leading to findings which were not achievable by SDR or NNP alone.

Future work can target several directions. As SDR-NNP showed that it is possible to learn sharpening methods for high-dimensional data, it is interesting to apply it to other domains beyond projection where such methods are used, *e.g.*, image segmentation, graph bundling, or data clustering and simplification. For the projection use-case, refining SDR-NNP's network architecture to accelerate its training is of high practical interest. Finally, deploying SDR-NNP as a daily tool for astronomers to analyze their million-sample datasets is a goal we want to pursue in the short term.

ACKNOWLEDGMENTS

This work is supported by the DSSC Doctoral Training Programme co-funded by the Marie Sklodowska-Curie COFUND project (DSSC 754315), and FAPESP grant 2020/13275-1, Brazil. The GALAH survey is based on observations made at the Australian Astronomical Observatory, under programmes A/2013B/13, A/2014A/25, A/2015A/19, A/2017A/18. We acknowledge the traditional owners of the land on which the AAT stands, the Gamilaraay people, and pay our respects to elders past and present. This work has made use of data from the European Space Agency (ESA) mission *Gaia* (https://www.cosmos.esa.int/gaia), processed by the *Gaia* Data Processing and Analysis Consortium (DPAC, https://www.cosmos.esa.int/web/gaia/dpac/consortium). Funding for the DPAC has been provided by national institutions, in particular the institutions participating in the *Gaia* Multilateral Agreement.

REFERENCES

Agarap, A. F. (2018). Deep learning using rectified linear units (ReLU). arXiv:1803.08375 [cs.NE].

Becker, M., Lippel, J., Stuhlsatz, A., and Zielke, T. (2020). Robust dimensionality reduction for data visualization with deep neural networks. *Graphical Models*, 108:101060.

Becker, R., Cleveland, W., and Shyu, M. (1996). The visual design and control of trellis display. *J Comp Graph Stat*, 5(2):123–155.

Behrisch, M., Blumenschein, M., Kim, N. W., Shao, L., El-Assady, M., Fuchs, J., Seebacher, D., Diehl, A., Brandes, U., Pfister, H., Schreck, T., Weiskopf, D., and Keim, D. A. (2018). Quality metrics for information visualization. *Comp Graph Forum*, 37(3):625–662.

Berkhin, P. (2006). A survey of clustering data mining techniques. In *Grouping Multidimensional Data*, pages 25–71. Springer.

Blanco, J. L. and Rai, P. K. (2014). nanoflann: a C++ header-only fork of FLANN, a library for nearest neighbor (NN) with kd-trees. https://github.com/jlblancoc/nanoflann.

Buder *et al.*, S. (2018). The GALAH Survey: Second data release. *Mon R R Astron Soc*, 478.

Chan, D., Rao, R., Huang, F., and Canny, J. (2018). T-SNE-CUDA: GPU-accelerated t-SNE and its applications to modern data. In *Proc. SBAC-PAD*, pages 330–338.

Cheng, Y. (1995). Mean shift, mode seeking, and clustering. *IEEE TPAMI*, 17(8):790–799.

Chollet, F. and others (2015). Keras. https://keras.io.

Comaniciu, D. and Meer, P. (2002). Mean shift: A robust approach toward feature space analysis. *IEEE TPAMI*, 24(5):603–619.

Cortez, P., Cerdeira, A., Almeida, F., Matos, T., and Reis, J. (2009). Modeling wine preferences by data mining from physicochemical properties. *Decis Support Sys*, 47(4):547–553.

Cunningham, J. and Ghahramani, Z. (2015). Linear dimensionality reduction: Survey, insights, and generalizations. *JMLR*, 16:2859–2900.

De Silva, V. and Tenenbaum, J. B. (2004). Sparse multidimensional scaling using landmark points. Technical report, Stanford University.

Donoho, D. L. and Grimes, C. (2003). Hessian eigenmaps: Locally linear embedding techniques for high-dimensional data. *PNAS*, 100(10):5591–5596.

El Helou, A. (2020). Sensor HAR recognition app. www.mathworks.com/matlabcentral/fileexchange/54138-sensor-har-recognition-app.

Engel, D., Hattenberger, L., and Hamann, B. (2012). A survey of dimension reduction methods for high-dimensional data analysis and visualization. In *Proc.*

IRTG Workshop, volume 27, pages 135–149. Schloss Dagstuhl.

Epanechnikov, V. (1969). Non-parametric estimation of a multivariate probability density. *Theor Probab Appl+*, 14.

Espadoto, M., Hirata, N., and Telea, A. (2020). Deep learning multidimensional projections. *Inform Visual*, 9(3):247–269.

Espadoto, M., Hirata, N., and Telea, A. (2021). Self-supervised dimensionality reduction with neural networks and pseudo-labeling. In *Proc. IVAPP*.

Espadoto, M., Martins, R., Kerren, A., Hirata, N., and Telea, A. (2019). Toward a quantitative survey of dimension reduction techniques. *IEEE TVCG*, 27(3):2153–2173.

Fisher, R. A. (1936). The use of multiple measurements in taxonomic problems. *Annals of eugenics*, 7(2):179–188.

Fukunaga, K. and Hostetler, L. (1975). The estimation of the gradient of a density function, with applications in pattern recognition. *IEEE Trans Inf Theor*, 21(1):32–40.

Gaia Collaboration (2016). The Gaia mission. *Astronomy & Astrophysics*, 595, A1.

Gaia Collaboration (2018). Gaia Data Release 2-Summary of the contents and survey properties. *Astronomy & Astrophysics*, 616, A1.

Guennebaud, G., Jacob, B., et al. (2010). Eigen v3. http://eigen.tuxfamily.org.

He, K., Zhang, X., Ren, S., and Sun, J. (2015). Delving deep into rectifiers: Surpassing human-level performance on ImageNet classification. In *Proc. ICCV*, pages 1026–1034.

Hinton, G. E. and Salakhutdinov, R. R. (2006). Reducing the dimensionality of data with neural networks. *Science*, 313(5786):504–507. Publisher: AAAS.

Hoffman, P. and Grinstein, G. (2002). A survey of visualizations for high-dimensional data mining. In *Information Visualization in Data Mining and Knowledge Discovery*, pages 47–82.

Hopkins, M., Reeber, E., Forman, G., and Suermondt, J. (1999). Spambase dataset. Hewlett-Packard Labs.

Hurter, C., Ersoy, O., and Telea, A. (2012). Graph bundling by kernel density estimation. *Comp Graph Forum*, 31(3):865–874.

Inselberg, A. and Dimsdale, B. (1990). Parallel coordinates: A tool for visualizing multi-dimensional geometry. In *Proc. IEEE Visualization*, pages 361–378.

Joia, P., Coimbra, D., Cuminato, J. A., Paulovich, F. V., and Nonato, L. G. (2011). Local affine multidimensional projection. *IEEE TVCG*, 17(12):2563–2571.

Jolliffe, I. T. (1986). Principal component analysis and factor analysis. In *Principal Component Analysis*, pages 115–128. Springer.

Kim, Y., Espadoto, M., Trager, S. C., Roerdink, J. B. T. M., and Telea, A. C. (2021a). SDR-NNP implementation and results. https://github.com/youngjookim/sdr-nnp.

Kim, Y., Telea, A., Trager, S., and Roerdink, J. B. T. M. (2021b). Visual cluster separation using high-dimensional sharpened dimensionality reduction. arXiv:2110.00317 [cs.CV].

Kingma, D. P. and Ba, J. (2014). Adam: A method for stochastic optimization. arXiv:1412.6980.

Kingma, D. P. and Welling, M. (2013). Auto-encoding variational bayes. *CoRR*, abs/1312.6114. eprint: 1312.6114.

Kohonen, T. (1997). *Self-organizing Maps*. Springer.

LeCun, Y. and Cortes, C. (2010). MNIST handwritten digits dataset. http://yann.lecun.com/exdb/mnist.

Lisitsyn, S., Widmer, C., and Garcia, F. J. I. (2013). Tapkee: An efficient dimension reduction library. *JMLR*, 14:2355–2359.

Liu, S., Maljovec, D., Wang, B., Bremer, P.-T., and Pascucci, V. (2015). Visualizing high-dimensional data: Advances in the past decade. *IEEE TVCG*, 23(3):1249–1268.

Maaten, L. v. d. (2014). Accelerating t-SNE using tree-based algorithms. *JMLR*, 15:3221–3245.

Maaten, L. v. d. and Hinton, G. (2008). Visualizing data using t-SNE. *JMLR*, 9:2579–2605.

Maaten, L. v. d. and Postma, E. (2009). Dimensionality reduction: A comparative review. Technical report, Tilburg Univ.

Martins, R. M., Minghim, R., Telea, A. C., and others (2015). Explaining neighborhood preservation for multidimensional projections. In *Proc. CGVC*, pages 7–14.

McInnes, L. and Healy, J. (2018). UMAP: Uniform manifold approximation and projection for dimension reduction. arXiv:1802.03426v1 [stat.ML].

Nonato, L. and Aupetit, M. (2018). Multidimensional projection for visual analytics: Linking techniques with distortions, tasks, and layout enrichment. *IEEE TVCG*.

Paulovich, F. V. and Minghim, R. (2006). Text map explorer: a tool to create and explore document maps. In *Proc. Information Visualisation*, pages 245–251. IEEE.

Paulovich, F. V., Nonato, L. G., Minghim, R., and Levkowitz, H. (2008). Least square projection: A fast high-precision multidimensional projection technique and its application to document mapping. *IEEE TVCG*, 14(3):564–575.

Pezzotti, N., Höllt, T., Lelieveldt, B., Eisemann, E., and Vilanova, A. (2016). Hierarchical stochastic neighbor embedding. *Comp Graph Forum*, 35(3):21–30.

Pezzotti, N., Lelieveldt, B., Maaten, L. v. d., Höllt, T., Eisemann, E., and Vilanova, A. (2017). Approximated and user steerable t-SNE for progressive visual analytics. *IEEE TVCG*, 23:1739–1752.

Pezzotti, N., Thijssen, J., Mordvintsev, A., Hollt, T., Lew, B. v., Lelieveldt, B., Eisemann, E., and Vilanova, A. (2020). GPGPU linear complexity t-SNE optimization. *IEEE TVCG*, 26(1):1172–1181.

Rao, R. and Card, S. K. (1994). The table lens: Merging graphical and symbolic representations in an interactive focus+context visualization for tabular information. In *Proc. ACM SIGCHI*, pages 318–322.

Rauber, P. E., Falcão, A. X., and Telea, A. C. (2017). Projections as visual aids for classification system design. *Inform Visual*, 17(4):282–305.

Roweis, S. T. and Saul, L. L. K. (2000). Nonlinear dimensionality reduction by locally linear embedding. *Science*, 290(5500):2323–2326.

Salton, G. and McGill, M. J. (1986). *Introduction to modern information retrieval*. McGraw-Hill.

Sorzano, C., Vargas, J., and Pascual-Montano, A. (2014). A survey of dimensionality reduction techniques. arXiv:1403.2877 [stat.ML].

Street, N., Wolberg, W., and Mangasarian, O. (1993). Nuclear feature extraction for breast tumor diagnosis. In *Biomedical image processing and biomedical visualization*, volume 1905, pages 861–870.

Tenenbaum, J. B., Silva, V. D., and Langford, J. C. (2000). A global geometric framework for nonlinear dimensionality reduction. *Science*, 290(5500):2319–2323.

Thoma, M. (2017). The Reuters dataset. https://martin-thoma.com/nlp-reuters.

Tinsley, B. (1980). Evolution of the stars and gas in galaxies. *Fundamentals of Cosmic Physics*, 5:287–388.

Torgerson, W. (1958). *Theory and Methods of Scaling*. Wiley.

Venna, J. and Kaski, S. (2006). Visualizing gene interaction graphs with local multidimensional scaling. In *Proc. ESANN*, pages 557–562.

Vito, S. D., Massera, E., Piga, M., Martinotto, L., and Francia, G. D. (2008). On field calibration of an electronic nose for benzene estimation in an urban pollution monitoring scenario. *Sensors and Actuators B: Chemical*, 129(2):750–757. https://archive.ics.uci.edu/ml/datasets/Air+Quality.

Wattenberg, M. (2016). How to use t-SNE effectively. https://distill.pub/2016/misread-tsne.

Xie, H., Li, J., and Xue, H. (2017). A survey of dimensionality reduction techniques based on random projection. arXiv:1706.04371 [cs.LG].

Xu, R. and Wunsch, D. (2005). Survey of clustering algorithms. *IEEE Transactions on Neural Networks*, 16(3):645–678.

Yates, A., Webb, A., Sharpnack, M., Chamberlin, H., Huang, K., and Machiraju, R. (2014). Visualizing multidimensional data with glyph SPLOMs. *Comp Graph Forum*, 33(3):301–310.

Yeh, I.-C. (1998). Modeling of strength of high-performance concrete using artificial neural networks. *Cement and Concrete Research*, 28(12):1797–1808.

Zhang, Z. and Wang, J. (2007). MLLE: Modified locally linear embedding using multiple weights. In *Proc. NIPS*, pages 1593–1600.

Zhang, Z. and Zha, H. (2004). Principal manifolds and nonlinear dimensionality reduction via tangent space alignment. *SIAM J Sci Comput*, 26(1):313–338.

APPENDIX

We next present tables containing full measurements
for the experiments described in Section 4.

Table 6: Metrics for SDR-NNP learned from LMDS, PCA, and t-SNE on the GALAH dataset for train and test samples for varying number of training epochs E ('early' indicates the early-stopping heuristic).

		LMDS			PCA			t-SNE		
Mode	Epochs	T	C	R	T	C	R	T	C	R
Train	early	0.802	0.877	0.676	0.787	0.853	0.668	0.789	0.870	0.638
	300	0.703	0.790	0.629	0.697	0.778	0.617	0.694	0.770	0.496
	1000	0.695	0.772	0.615	0.693	0.762	0.607	0.692	0.748	0.481
	3000	0.692	0.756	0.600	0.693	0.756	0.601	0.691	0.734	0.447
Test	early	0.775	0.862	0.601	0.754	0.828	0.592	0.756	0.853	0.574
	300	0.667	0.768	0.558	0.660	0.759	0.544	0.652	0.755	0.470
	1000	0.661	0.749	0.547	0.658	0.746	0.539	0.642	0.734	0.449
	3000	0.657	0.737	0.534	0.655	0.739	0.539	0.641	0.720	0.416

Table 7: Metrics for SDR-NNP learned from LMDS, PCA, and t-SNE for different numbers of iterations t and different datasets. SDR-NNP parameters used: $\alpha = 0.1$, $E = 1000$, *medium* network size. NH values not available for the Air Quality and Concrete datasets since these are not labeled.

		LMDS				PCA				t-SNE			
Dataset	SDR iterations	T	C	R	NH	T	C	R	NH	T	C	R	NH
Air Quality	0	0.941	0.992	0.970		0.940	0.992	0.966		0.996	0.996	0.654	
	4	0.962	0.979	0.963		0.956	0.979	0.963		0.951	0.939	0.396	
	8	0.954	0.970	0.952		0.942	0.970	0.948		0.945	0.938	0.313	
	12	0.949	0.970	0.952		0.945	0.970	0.936		0.942	0.942	0.365	
	16	0.950	0.968	0.943		0.948	0.967	0.930		0.940	0.933	0.317	
	20	0.954	0.968	0.939		0.949	0.967	0.917		0.943	0.939	0.334	
Concrete	0	0.940	0.979	0.744		0.934	0.977	0.736		0.996	0.992	0.479	
	4	0.938	0.958	0.631		0.934	0.957	0.627		0.952	0.929	0.145	
	8	0.912	0.944	0.560		0.906	0.943	0.564		0.927	0.918	0.140	
	12	0.895	0.941	0.556		0.865	0.932	0.558		0.912	0.913	0.167	
	16	0.884	0.938	0.554		0.872	0.932	0.555		0.904	0.914	0.118	
	20	0.876	0.935	0.560		0.874	0.934	0.569		0.890	0.910	0.109	
Reuters	0	0.817	0.895	0.755	0.724	0.817	0.888	0.754	0.727	0.956	0.960	0.609	0.856
	4	0.835	0.913	0.752	0.747	0.833	0.901	0.745	0.743	0.957	0.951	0.405	0.855
	8	0.858	0.915	0.713	0.775	0.854	0.906	0.706	0.765	0.950	0.910	0.258	0.845
	12	0.883	0.909	0.693	0.803	0.883	0.904	0.687	0.802	0.915	0.855	0.078	0.820
	16	0.884	0.910	0.691	0.810	0.882	0.907	0.689	0.804	0.893	0.849	0.102	0.813
	20	0.882	0.907	0.691	0.800	0.883	0.907	0.691	0.810	0.893	0.852	0.113	0.820
Spambase	0	0.740	0.909	0.529	0.852	0.747	0.912	0.513	0.849	0.954	0.958	0.408	0.914
	4	0.737	0.881	0.463	0.843	0.743	0.877	0.471	0.841	0.873	0.899	0.294	0.882
	8	0.723	0.855	0.403	0.838	0.712	0.848	0.383	0.834	0.793	0.845	0.312	0.866
	12	0.711	0.845	0.379	0.829	0.704	0.838	0.348	0.830	0.754	0.841	0.324	0.850
	16	0.701	0.837	0.370	0.828	0.701	0.837	0.322	0.830	0.744	0.834	0.332	0.845
	20	0.710	0.840	0.351	0.833	0.709	0.838	0.311	0.836	0.739	0.828	0.283	0.848
Wisconsin	0	0.895	0.959	0.926	0.941	0.896	0.959	0.928	0.943	0.950	0.939	0.679	0.976
	4	0.892	0.915	0.901	0.953	0.888	0.915	0.903	0.958	0.897	0.878	0.557	0.957
	8	0.804	0.857	0.785	0.925	0.805	0.856	0.785	0.925	0.814	0.816	0.256	0.925
	12	0.790	0.849	0.735	0.930	0.787	0.848	0.736	0.930	0.794	0.805	0.393	0.932
	16	0.780	0.847	0.721	0.916	0.780	0.844	0.718	0.922	0.779	0.820	0.432	0.913
	20	0.775	0.842	0.707	0.922	0.776	0.841	0.705	0.920	0.778	0.829	0.457	0.921
Wine	0	0.864	0.973	0.839	0.667	0.869	0.972	0.806	0.678	0.986	0.976	0.656	0.702
	4	0.867	0.932	0.709	0.669	0.864	0.930	0.686	0.665	0.911	0.894	0.341	0.673
	8	0.843	0.916	0.676	0.661	0.843	0.917	0.683	0.661	0.869	0.876	0.283	0.665
	12	0.840	0.904	0.646	0.665	0.841	0.905	0.653	0.668	0.846	0.864	0.289	0.668
	16	0.845	0.901	0.625	0.664	0.843	0.903	0.635	0.663	0.845	0.865	0.321	0.664
	20	0.842	0.899	0.579	0.659	0.846	0.898	0.593	0.664	0.845	0.868	0.292	0.666

Table 8: Metrics for SDR-NNP learned from LMDS, PCA, and t-SNE for different learning rates α. SDR-NNP parameters: $t = 10$ iterations, $E = 1000$ epochs, *medium* network. NH values not available for the Air Quality and Concrete datasets since these are not labeled.

		LMDS				PCA				t-SNE			
Dataset	Learning Rate	T	C	R	NH	T	C	R	NH	T	C	R	NH
Air Quality	0.01	0.971	0.990	0.969		0.968	0.990	0.964		0.958	0.926	0.052	
	0.05	0.976	0.983	0.963		0.973	0.984	0.964		0.938	0.911	0.175	
	0.1	0.951	0.969	0.948		0.940	0.969	0.941		0.943	0.939	0.378	
	0.2	0.866	0.941	0.911		0.862	0.928	0.905		0.824	0.876	0.635	
Concrete	0.01	0.959	0.983	0.731		0.950	0.979	0.721		0.994	0.988	0.486	
	0.05	0.932	0.957	0.601		0.929	0.953	0.601		0.947	0.929	0.219	
	0.1	0.870	0.933	0.578		0.889	0.935	0.583		0.913	0.918	0.057	
	0.2	0.858	0.920	0.540		0.859	0.921	0.542		0.857	0.900	0.223	
Reuters	0.01	0.822	0.900	0.758	0.729	0.821	0.892	0.755	0.730	0.956	0.960	0.608	0.853
	0.05	0.839	0.913	0.737	0.745	0.838	0.903	0.735	0.745	0.955	0.949	0.386	0.849
	0.1	0.870	0.910	0.698	0.783	0.871	0.905	0.693	0.790	0.936	0.885	0.159	0.829
	0.2	0.866	0.902	0.700	0.784	0.867	0.903	0.693	0.785	0.890	0.848	0.096	0.815
Spambase	0.01	0.755	0.911	0.527	0.860	0.756	0.915	0.523	0.852	0.958	0.942	0.383	0.905
	0.05	0.775	0.893	0.415	0.840	0.787	0.894	0.426	0.858	0.851	0.874	0.261	0.874
	0.1	0.712	0.843	0.380	0.832	0.704	0.839	0.367	0.828	0.769	0.848	0.341	0.863
	0.2	0.604	0.667	0.265	0.760	0.606	0.671	0.263	0.764	0.635	0.676	0.317	0.802
Wisconsin	0.01	0.900	0.960	0.932	0.947	0.898	0.960	0.932	0.949	0.955	0.941	0.635	0.966
	0.05	0.868	0.885	0.869	0.946	0.874	0.890	0.870	0.941	0.876	0.861	0.597	0.948
	0.1	0.803	0.856	0.757	0.928	0.800	0.851	0.753	0.929	0.802	0.841	0.494	0.927
	0.2	0.717	0.764	0.693	0.905	0.718	0.758	0.684	0.918	0.725	0.749	0.596	0.909
Wine	0.01	0.895	0.972	0.811	0.674	0.898	0.971	0.783	0.681	0.983	0.951	0.448	0.696
	0.05	0.914	0.944	0.734	0.671	0.920	0.945	0.714	0.670	0.927	0.862	0.135	0.670
	0.1	0.837	0.913	0.672	0.658	0.848	0.913	0.672	0.664	0.864	0.882	0.250	0.661
	0.2	0.739	0.821	0.479	0.653	0.742	0.825	0.484	0.644	0.744	0.808	0.404	0.646